Supplementary Fig. 1

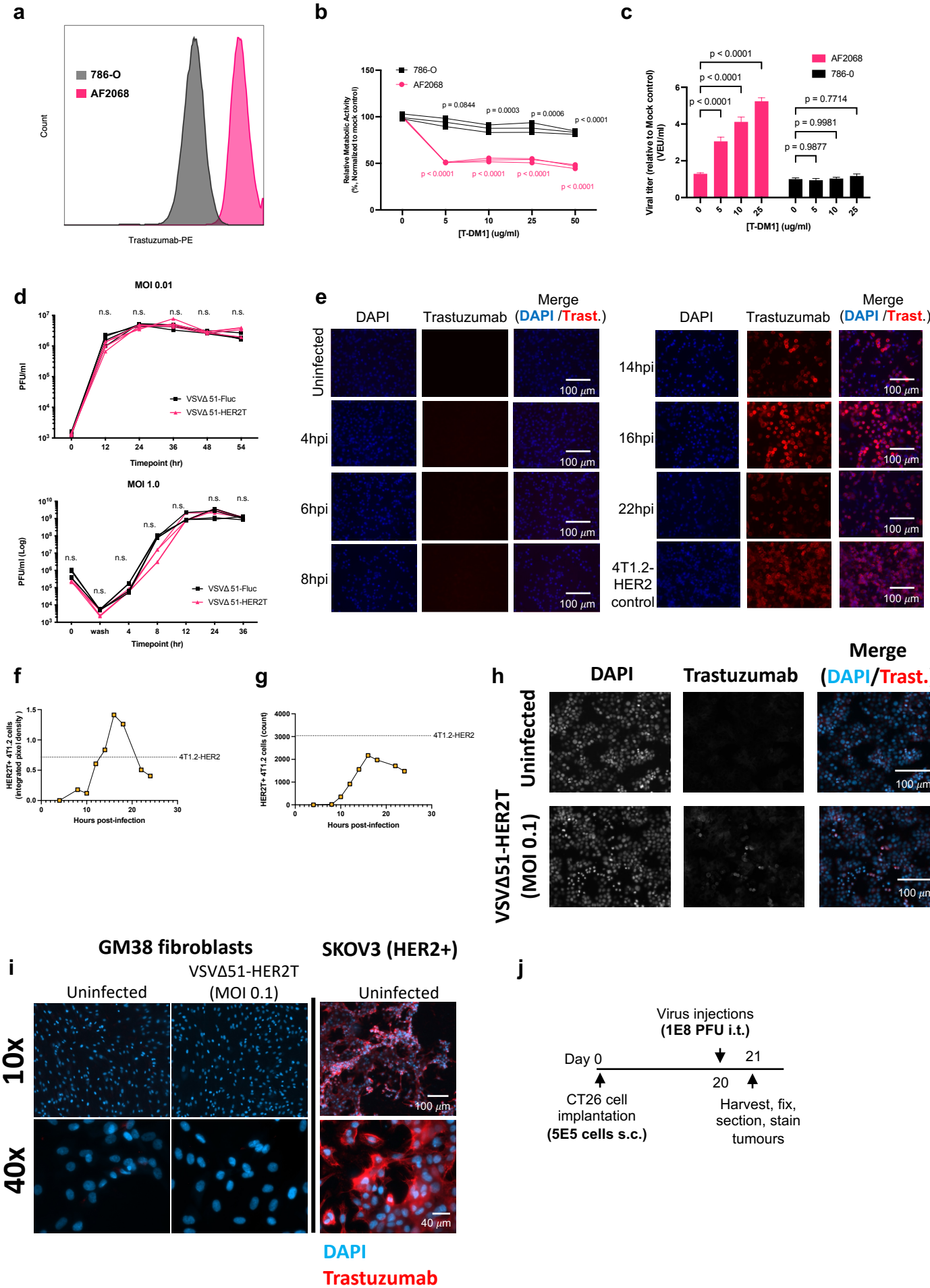

Supplementary Fig. 1: Target-selectivity of trastuzumab and VSVΔ51-HER2T. (a) Single-cell suspensions of 786-O and AF2068 cell lines were stained with trastuzumab as a primary antibody (1:1000) then incubated with anti-human IgG-PE secondary antibody. Data were acquired by flow cytometry to detect Trastuzumab-PE signal. (b) 786-O and AF2068 cells were treated in 24-well plates with T-DM1 at the indicated concentrations for 2 h. Supernatants were removed and cells were washed and replenished with fresh medium to remove excess unbound ADC. Cell viability was assessed by AlamarBlue, 48 h post-treatment, and normalized to untreated controls. Shown are mean ± SEM, $n = 3$, *P*-value calculated by one-way ANOVA relative to untreated control with Dunnett correction for multiple comparisons. (c) Cells were treated as in (b) then infected with MOI 0.001 VSVΔ51-Fluc. Viral supernatant was quantified 48 hpi by high-throughput luciferase titering. Shown are mean ± SEM, $n = 3$, *P*-value calculated by one-way ANOVA relative to untreated control with Dunnett correction for multiple comparisons. (d) Overview of VSVΔ51 multi-step (top, MOI 0.01) and single-step (bottom, MOI 1.0) VSVΔ51 growth curves; 4T1.2 cells were seeded in 24-well plates at 2×10^5 cells per well and incubated overnight. Cells were infected with VSVΔ51-HER2T or VSVΔ51-Fluc and incubated. Viral supernatant was collected at the indicated timepoints post-infection, including the wash where "w" is indicated, and viral titer was quantified by plaque assay. Shown are mean ± SEM, $n = 3$, *P*-value calculated by two-tailed unpaired t-test at each timepoint between both VSVΔ51 variants. (e) 4T1.2 cells were seeded on glass coverslips and infected with VSVΔ51-HER2T MOI 0.1, then incubated at 37^0C uninfected 4T1.2-HER2T were stained as a control. Cells were fixed with 4% PFA at the indicated timepoints post-infection and stained then mounted and imaged at 20× magnification. Similar results were observed in 3 independent experiments. (f) Total staining intensity was calculated using ImageJ, and (g) trastuzumab-positive cells were counted. (h) Human HT29 cells were seeded on glass coverslips, after which cells were infected with VSVΔ51-HER2T at an MOI of 0.1. Cells were fixed and stained 24 hpi using trastuzumab as a primary antibody (1:1000) and imaged using a Zeiss AxioImage.M2 microscope at 20× magnification. Similar results were observed in 3 independent experiments, with similar HER2-low human cell lines. (i) Normal human fibroblasts GM38 cells were seeded on glass coverslips then infected with VSVΔ51-HER2T an MOI 0.1. Cells were fixed and stained 24 hpi then imaged at the indicated magnifications. SKOV3 cells were used as HER2+ controls. Similar results were observed in 2 independent experiments. (j) Balb/c ($n = 3$) mice were implanted with subcutaneous bilateral CT26 tumours in the flanks. Upon reaching ~400 mm^3 (day 20 post-implantation) tumours were injected with VSVΔ51-HER2T (right hand right) or VSVΔ51-GFP as a control (left hand side), at 1×10^8 PFU. Tumours were excised 24 h post-implantation, flash frozen in O.C.T. medium, sectioned, fixed in 4% PFA, and stained. Source data are provided as a Source Data file.

Supplementary Fig. 2

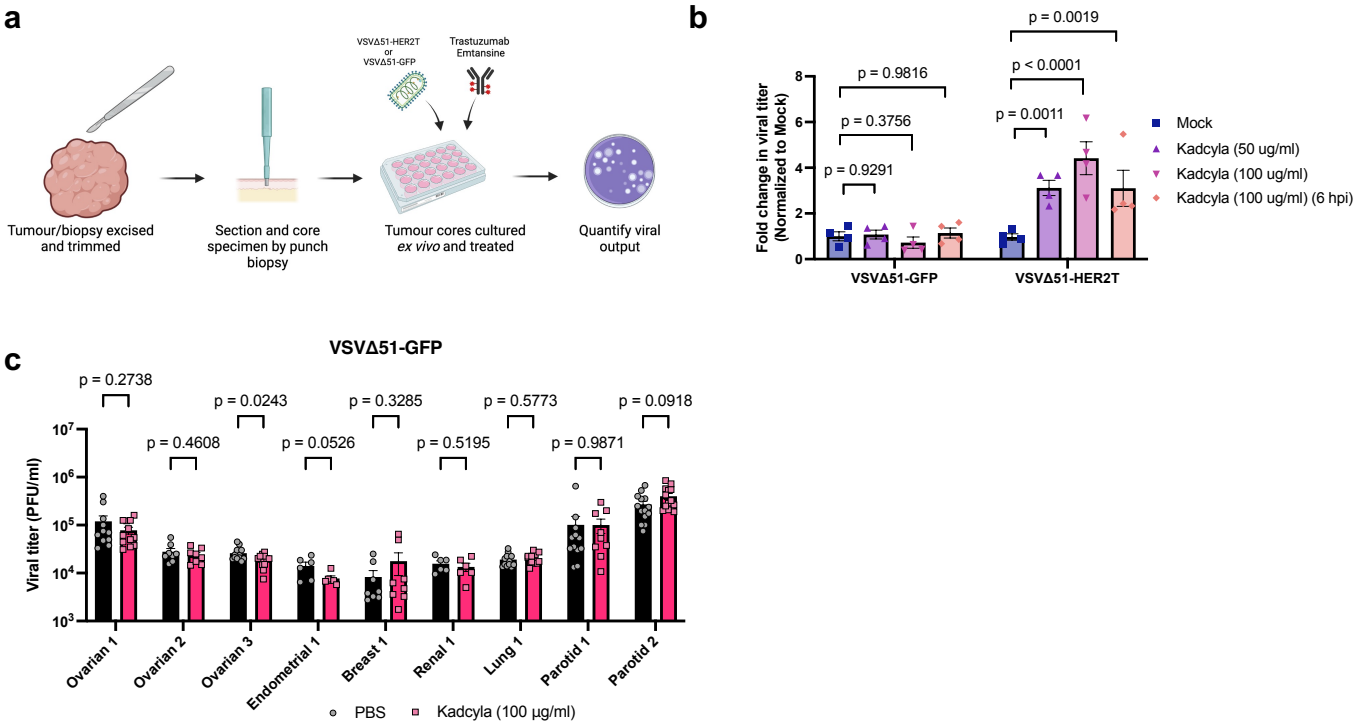

Supplementary Fig. 2: VSVΔ51-HER2T delivers the target antigen for T-DM1 leading to enhanced viral output in *ex vivo* patient tumours. (a) Schematic highlighting the process of generating and treating tumour cores. (b) Cores from CT26 tumours were infected and treated as indicated. 48 hpi viral titer in the core supernatants was quantified and plotted. Shown are mean ± SEM, $n = 4$ cores, *P*-value calculated by two-way ANOVA with Dunnett correction for multiple comparisons. (c) Patient tumour cores were infected with VSVΔ51-GFP and co-treated with T-DM1 or mock (PBS) as indicated. Viral titer in supernatants was quantified 48 hpi. (mean ± SEM, $n = 4$-14 cores, *P*-value calculated by multiple unpaired two-tailed t-tests; Endometrial 1 $n = 4$, Renal 1 $n = 6$, Ovarian 2 and Breast 1 $n = 8$, Parotid 2 $n = 14$, all others $n = 12$). Source data are provided as a Source Data file.

Supplementary Fig. 3

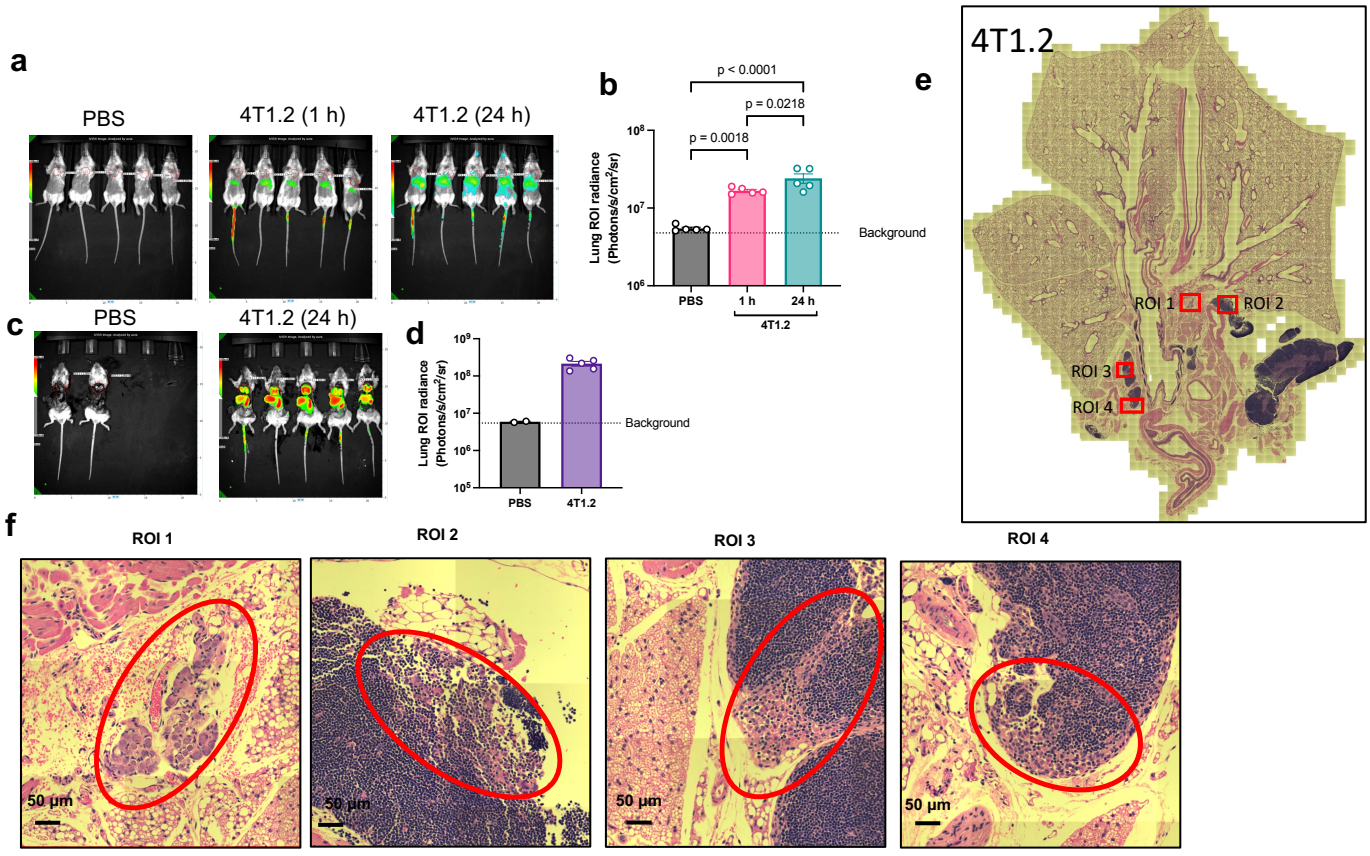

Supplementary Fig. 3: 4T1.2 cells injected intravenously establish microscopic lesions within the lungs within 24 h. (a) 4T1.2 cells were injected intravenously, via tail vein, into BALB/c mice. Control mice were injected with PBS. Cells were stained with an infrared dye. Mice underwent fluorescence IVIS imaging at 1 h and 24 h post-injection, at excitation 710 nm and emission 760 nm. (b) Quantification of red lung ROIs from (a) (mean ± SEM, $n = 5$ mice, p-value calculated by one way ANOVA with Fisher's LSD test). (c) Mice from (a) were euthanized, chest cavities were opened, and ribcages removed to expose lungs for subsequent IVIS imaging. (d) Quantification of red lung ROIs from (c) (mean ± SEM, $n = 2$-5 mice). (e) Lungs from (c) were perfused, fixed by formalin instillation, and processed for sectioning and H&E staining. Lung sections underwent histological evaluation by a pathologist (blinded). (f) Red ROIs (1-4) indicate representative microscopic 4T1.2 lesions. Source data are provided as a Source Data file.

Supplementary Fig. 4

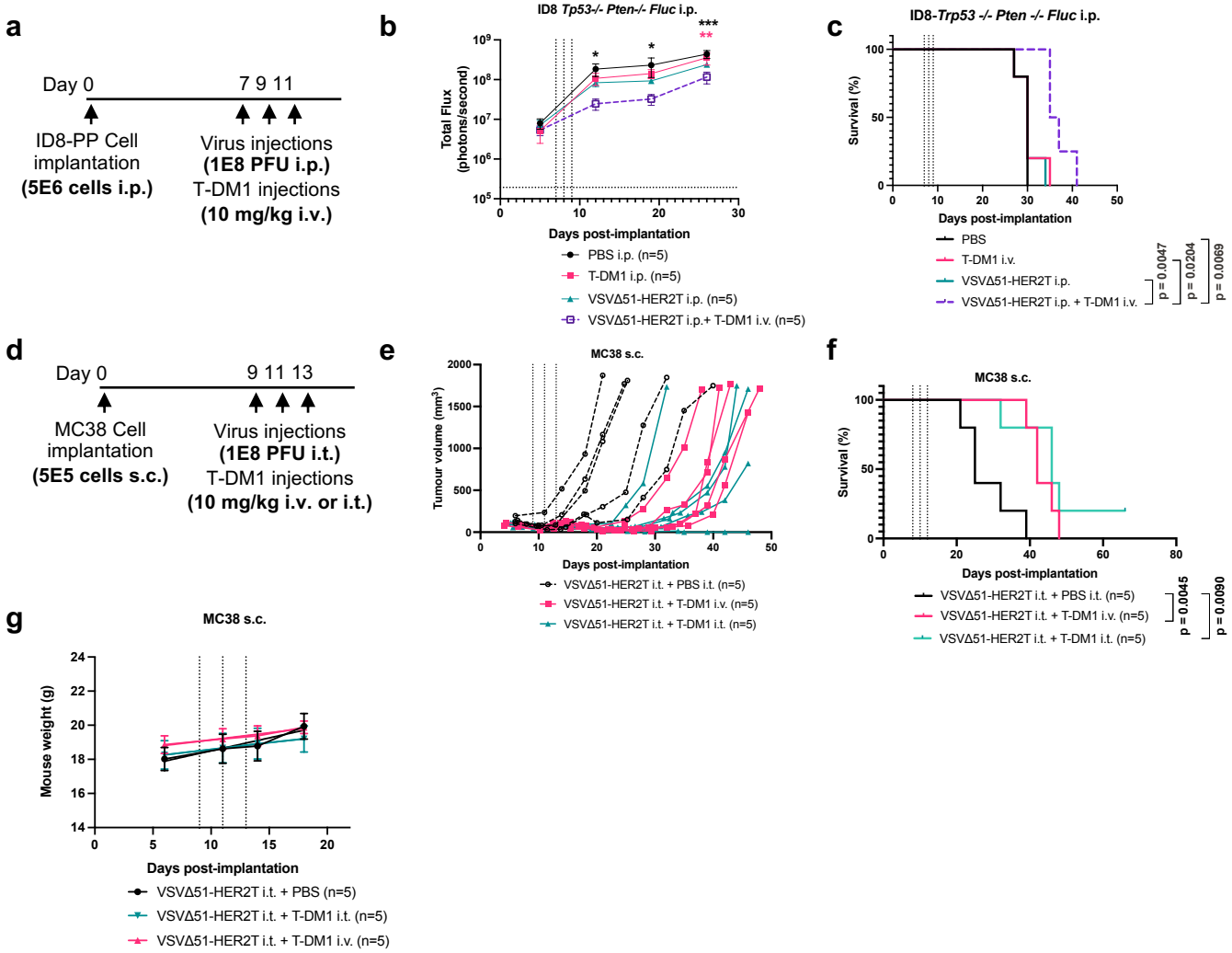

Supplementary Fig. 4: VSVΔ51-HER2T delivers the target antigen for T-DM1 and yields combinatorial efficacy in syngeneic murine tumour models. (a) Experimental overview: 5×10^6 ID8 *Tp53-/- Pten-/-* Fluc cells were implanted i.p. into wildtype C57BL/6 mice on D0 and treated on D7, D9, and D11 as indicated. (b) Mice were treated i.p. as indicated by the dotted lines. Mice underwent 4 rounds of IVIS imaging, 1 week apart, beginning on D5. Total flux was calculated and plotted. Shown are mean ± SEM, $n = 5$ mice per group, * $P < 0.05$, *** $P < 0.001$; comparison between VSVΔ51-HER2T+T-DM1 and whichever group the asterisk colour matches, by two-way ANOVA with Fisher's LSD test. Exact *P*-values are provided in the Source Data file. (c) Mice from (d-e) were monitored for overall survival; (d) Experimental overview: 5×10^5 MC38 cells were implanted s.c. into the right flanks of wildtype C57BL/6 mice on D0, and treated on D9, D11, and D13 as indicated. (e) Tumour volumes were measured by electronic calipers and (f) overall survival was monitored. (g) Mouse weights from (d) were measured (mean ± SEM, $n = 5$ mice). Source data are provided as a Source Data file.

Supplementary Fig. 5

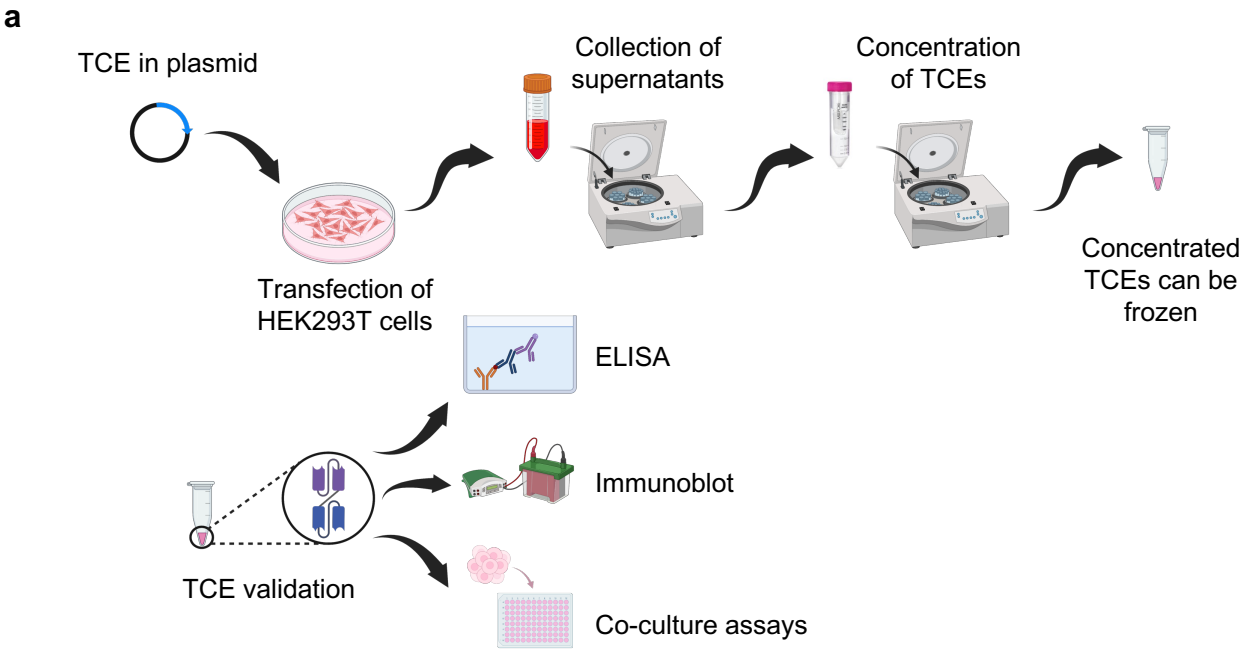

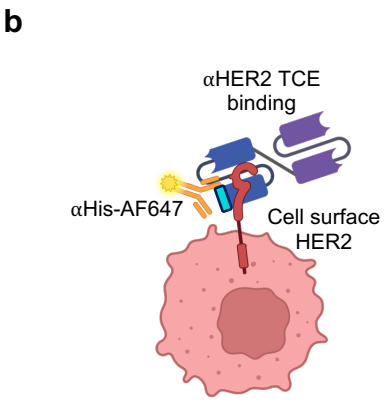

Supplementary Fig. 5: TCE generation and binding. (a) Schematic highlighting the generation and purification of TCEs *in vitro* (b) Overview of the TCE binding assay.

Supplementary Fig. 6

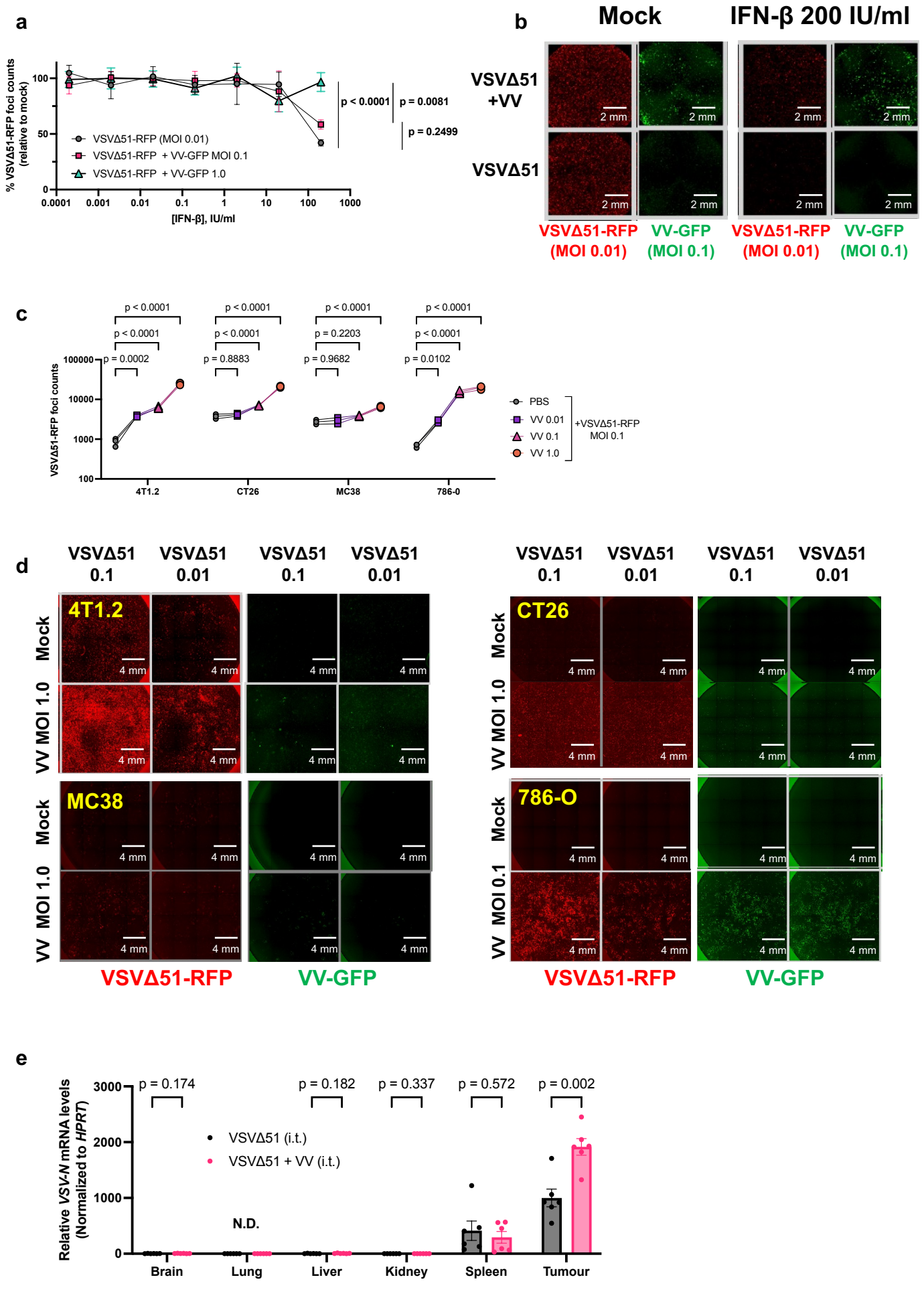

Supplementary Fig. 6: Determining the effects of IFNβ and VV on VSVΔ51 infection. (a) Vero cells seeded in 96-well plates at 2.5×10^4 cells per well, and were infected with VSVΔ51-RFP at an MOI of 0.01 ± co-infection with VV-GFP at the indicated MOI. IFNβ was added 2 hpi. RFP and GFP counts were quantified 48 hpi using the Cellomics ArrayScan. Shown are mean ± SEM, $n = 3$, *P*-value calculation by one-way ANOVA with Tukey's correction for multiple comparisons. (b) RFP (VSVΔ51 foci) and GFP (VV foci) images from (a), at 0 and 200 IU/ml IFNβ, imaged at 2.5× magnification. (c) The indicated cell lines were seeded in 24-well plates and infected with VSVΔ51-RFP at the indicated MOI ± co-infection with VV-GFP at the indicated MOI. RFP foci counts were quantified 48 hpi as in (a). Shown are mean ± SEM, $n = 3$, *P*-value calculated by two-way ANOVA relative to Mock (PBS), with Dunnett correction for multiple comparisons. (d) RFP (VSVΔ51 foci) and GFP (VV foci) images from, imaged at 2.5× magnification. (c). (e) BALB/c mice bearing CT26 tumours were injected i.t. with the indicated viruses (1×10^8 PFU VSVΔ51; 1×10^7 PFU VV). Mice were euthanized 48 hpi; tumours and organs were harvested and snap frozen. *VSV-N* mRNA expression was measured in different organs to assess the biodistribution of VSVΔ51 by qRT-PCR. Shown are mean ± SEM, $n = 3$ mice per group, *P*-value calculated by Student's t-test. (N.D. not detected) Source data are provided as a Source Data file.

Supplementary Fig. 7

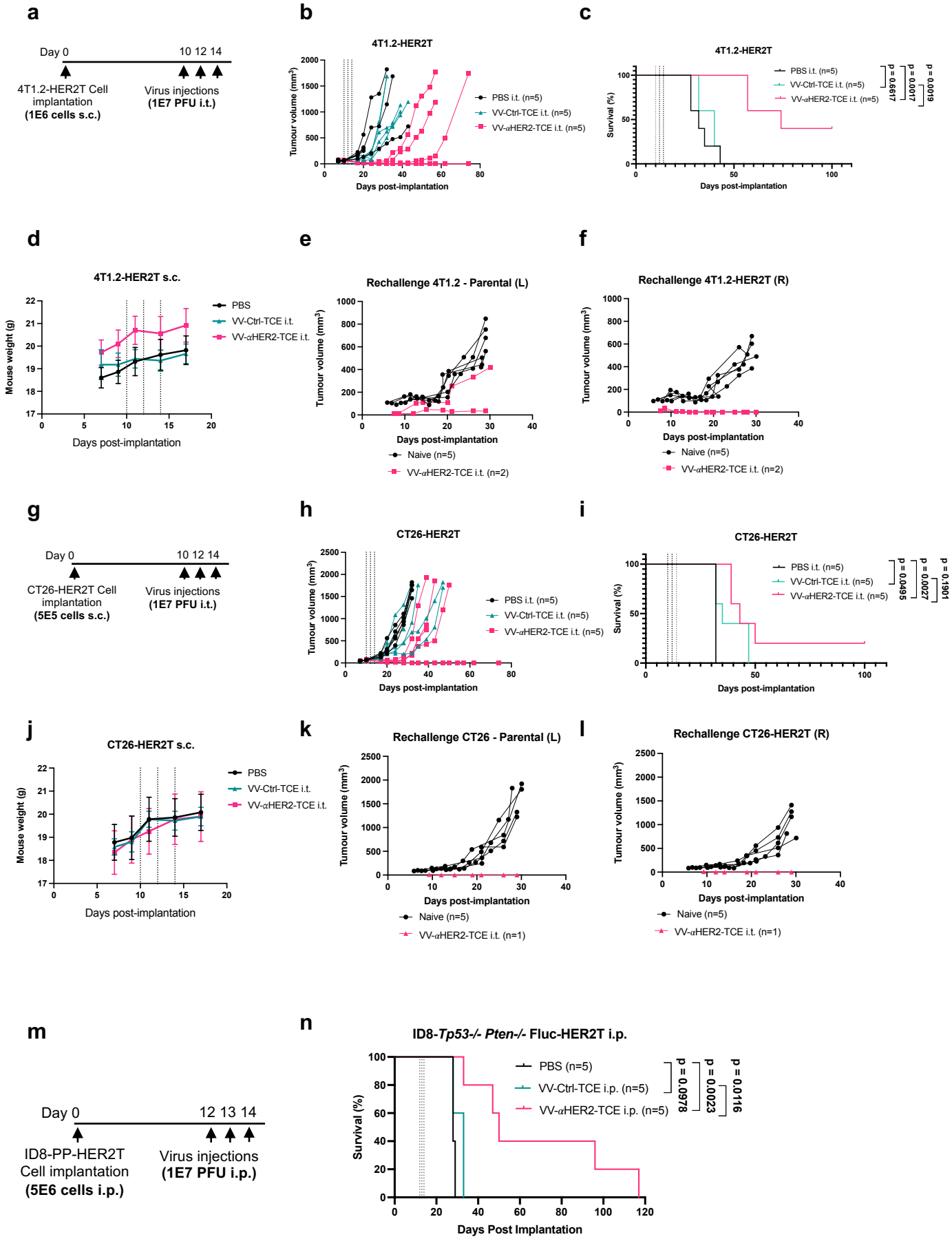

Supplementary Fig. 7: Treatment of syngeneic murine HER2T+ tumour models with VV-αHER2-TCE leads to efficacy. (a) Experimental overview: 1×10^6 4T1.2-HER2T cells were implanted s.c. in the right flank in BALB/c mice, followed by i.t. treatments as indicated. (b) Tumours volumes from (a) were monitored (mean ± SEM, $n = 5$ mice per group). (c) Overall survival from (a) was monitored. (d) Mouse weights from (a). (e-f) Cured mice from (a-c) were re-challenged with bilateral s.c. tumours, (e) parental 4T1.2 or (f) 4T1.2-HER2T as indicated. Naïve mice were challenged with bilateral s.c. tumours as indicated, and tumour volumes were monitored. (g) Experimental overview: 5×10^5 CT26-HER2T cells were implanted s.c. in the right flank in BALB/c mice, followed by i.t. treatments as indicated (h) Tumours volumes from (f) were monitored (mean ± SEM, $n = 5$ mice per group). (i) Overall survival from (g) was monitored. (j) Mouse weights from (g). (k-l) Cured mice from (g-i) were re-challenged with bilateral s.c. tumours, (k) parental CT26 or (l) CT26-HER2T as indicated. Naïve mice were challenged with bilateral s.c. tumours as indicated, and tumour volumes were monitored. (m) Experimental overview: 5×10^6 ID8-PP-HER2T cells were implanted i.p. in C57BL/6 mice, followed by i.p. treatments as indicated. (n) Overall survival from (k) was monitored. Source data are provided as a Source Data file.

Supplementary Fig. 8

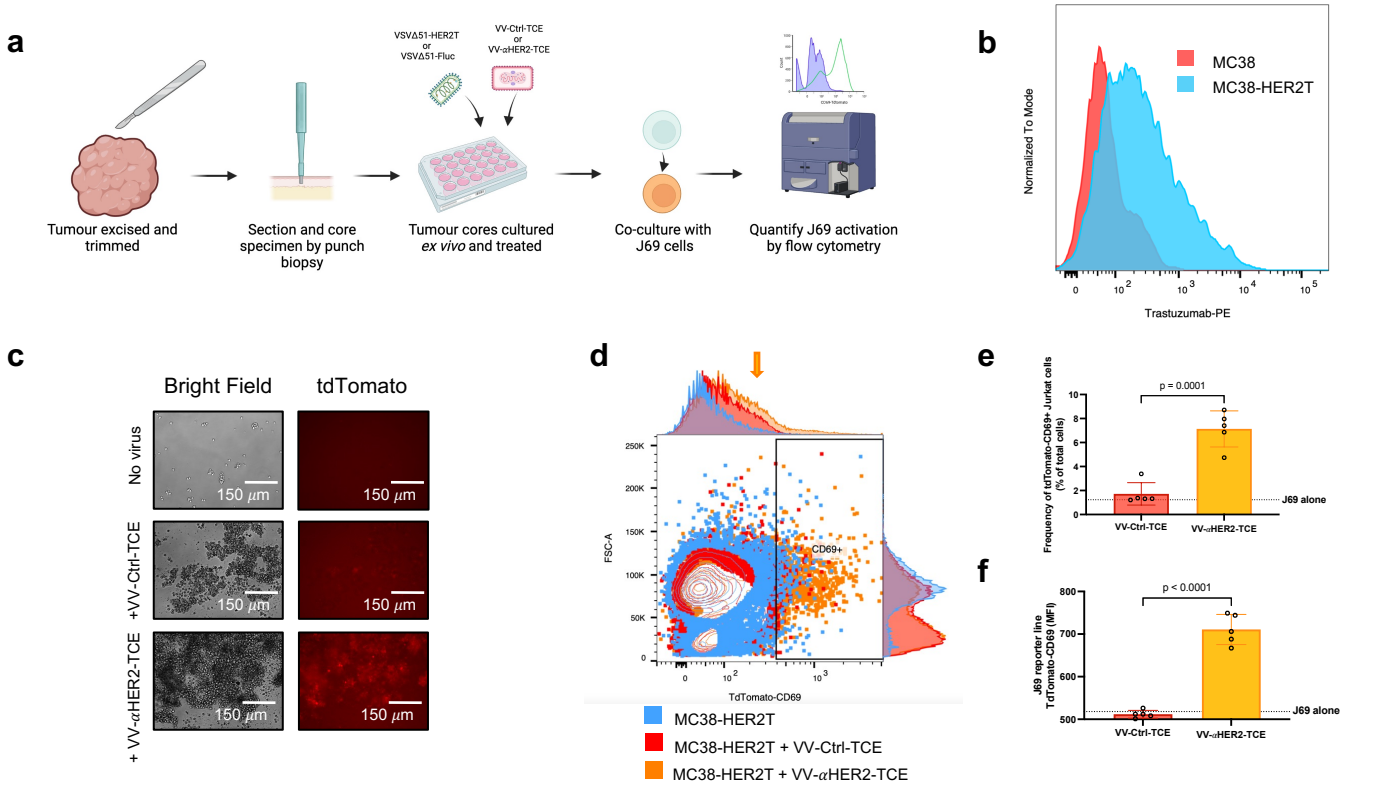

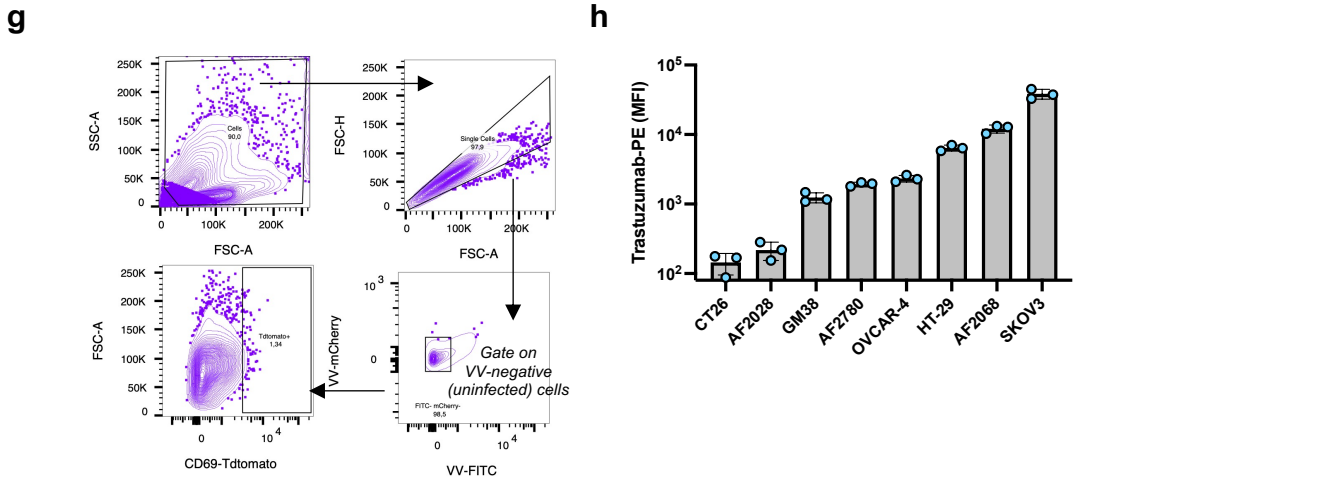

Supplementary Fig. 8: Validation of tumour core, co-culture assays, and flow cytometry. (a) Schematic highlighting the process of acquiring, processing, and analyzing tumour core specimens. (b) MC38 and MC38-HER2T cells were analyzed by flow cytometry for trastuzumab-PE binding. (c) MC38-HER2T tumour cores were co-cultured with J69 cells *ex vivo* followed treatment as indicated. Images of J69 cells were acquired using a EVOS M5000 microscope (10× magnification). (d) J69 cells from (c) were isolated, and TdTomato signal was quantified by flow cytometric analysis. The orange arrow indicates the shift in TdTomato signal followed treatment with VV-*α*HER2-TCE. (e) Frequency of TdTomato J69 cells and (f) MFI of TdTomato + J69 cells were quantified. Shown are mean ± SEM, $n = 5$ cores per group; *P*-value was calculated by unpaired two-tailed t-test. (g) Gating strategy for identification of TdTomato + J69 cells in (d-f). (h) Quantification of cell surface HER2 by flow cytometric analysis, using trastuzumab (1:1000) as a primary antibody. Shown are mean ± SEM, $n = 3$ biological replicates per cell line. Source data are provided as a Source Data file.

Supplementary Fig. 9

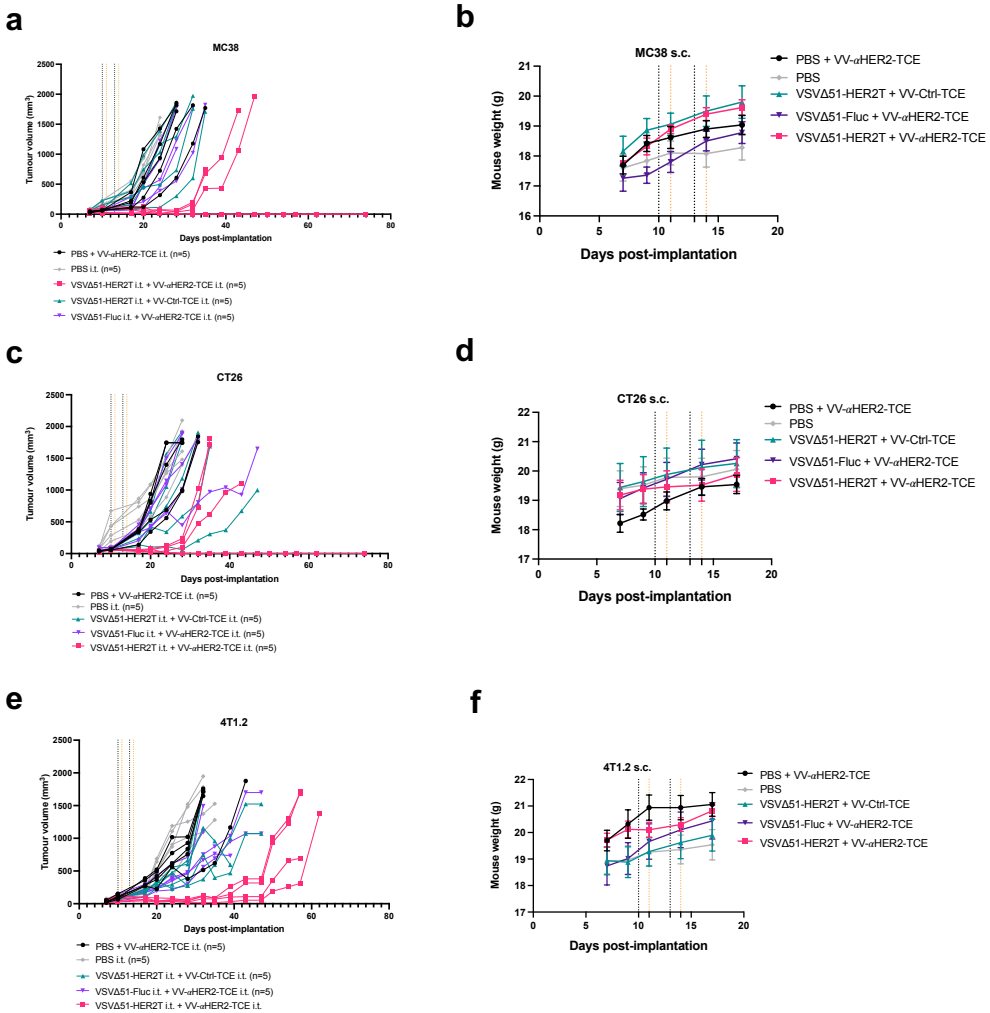

Supplementary Fig. 9: *In vivo* study designs and tumour volumes. (a) MC38 s.c. tumour volumes were measured and plotted for individual mice. Treatments are indicated by the dotted lines. (b) Mouse weights from (a) were monitored. Shown are mean ± SEM, $n = 5$ per group. (c) CT26 s.c. tumour volumes were measured and plotted for individual mice. Treatments are indicated by the dotted lines. (d) Mouse weights from (c) were monitored. Shown are mean ± SEM, $n = 5$ per group. (e) 4T1.2 s.c. tumour volumes were measured and plotted for individual mice. Treatments are indicated by the dotted lines. (f) Mouse weights from (e) were monitored. (mean ± SEM, $n = 5$ per group). Source data are provided as a Source Data file.

Supplementary Fig. 10

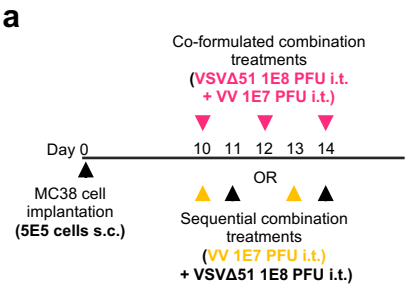

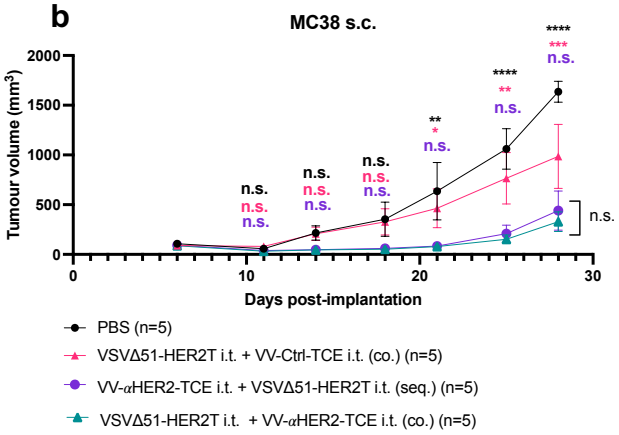

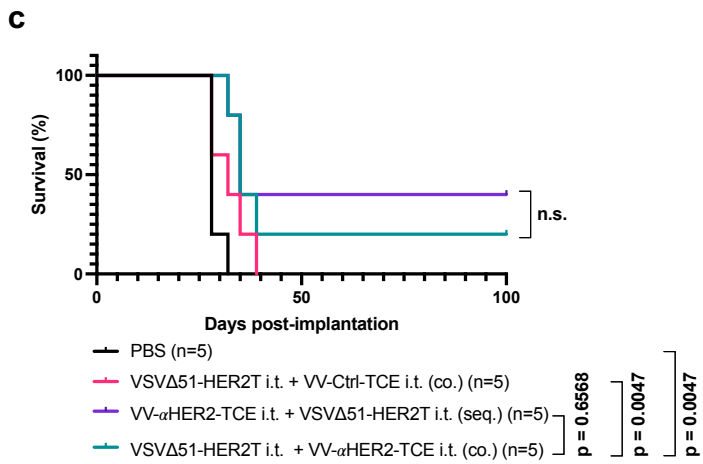

d

Day 6		
PBS	ns	0.9153
VSVΔ51-HER2T i.t. + VV-Ctrl-TCE i.t. (co.)	ns	0.9926
VSVΔ51-HER2T i.t. + VV-αHER2-TCE i.t. (seq.)	ns	0.9835

Day 11		
PBS	ns	0.8868
VSVΔ51-HER2T i.t. + VV-Ctrl-TCE i.t. (co.)	ns	0.7864
VSVΔ51-HER2T i.t. + VV-αHER2-TCE i.t. (seq.)	ns	0.9696

Day 14		
PBS	ns	0.3519
VSVΔ51-HER2T i.t. + VV-Ctrl-TCE i.t. (co.)	ns	0.3765
VSVΔ51-HER2T i.t. + VV-αHER2-TCE i.t. (seq.)	ns	0.9978

Day 18		
PBS	ns	0.099
VSVΔ51-HER2T i.t. + VV-Ctrl-TCE i.t. (co.)	ns	0.1333
VSVΔ51-HER2T i.t. + VV-αHER2-TCE i.t. (seq.)	ns	0.9645

Day 21		
PBS	**	0.0027
VSVΔ51-HER2T i.t. + VV-Ctrl-TCE i.t. (co.)	*	0.0366
VSVΔ51-HER2T i.t. + VV-αHER2-TCE i.t. (seq.)	ns	0.9784

Day 25		
PBS	****	<0.0001
VSVΔ51-HER2T i.t. + VV-Ctrl-TCE i.t. (co.)	**	0.001
VSVΔ51-HER2T i.t. + VV-αHER2-TCE i.t. (seq.)	ns	0.7565

Day 28		
PBS	****	<0.0001
VSVΔ51-HER2T i.t. + VV-Ctrl-TCE i.t. (co.)	***	0.0004
VSVΔ51-HER2T i.t. + VV-αHER2-TCE i.t. (seq.)	ns	0.5402

Supplementary Fig. 10: Validation of the co-formulated virus co-injections *in vivo.* (a) Experimental overview: 5×10^5 MC38 cells were implanted s.c. in the right flank of C57BL/6 mice. Mice were treated as indicated with the dual-virus combination; pink arrows indicate treatment with the co-formulated single-injection of both viruses. Orange and black arrows indicate sequential treatment with each virus. (b) Tumour volumes (mean ± SEM, $n = 5$ per group; p-values calculated by two-way ANOVA relative to the co-injection group with Fisher's LSD test; colour of the asterisks match the colour of the treatment group being compared) and (c) overall survival were monitored. (d) P-values were calculated by two-way ANOVA using tumour volume data from (b), all compared to VSVΔ51-HER2T i.t. + VV-αHER2-TCE i.t. co-formulated injection (teal curve). Source data are provided as a Source Data file.

Supplementary Fig. 11

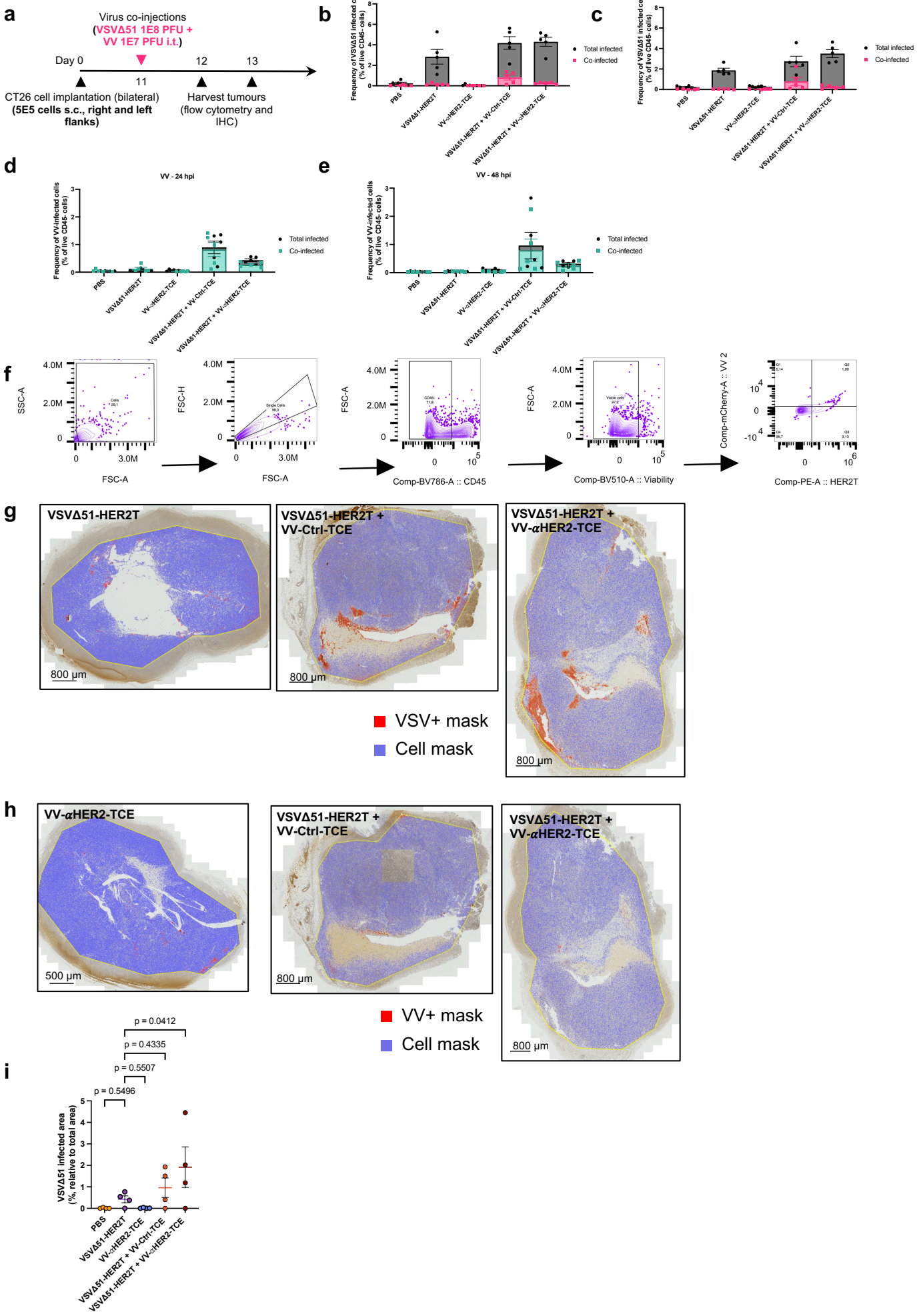

Supplementary Fig. 11: Assessment of CT26 tumour infection at 24 and 48 h post-injection. (a) Experimental overview: 5×10^5 CT26 cells were implanted bilaterally in BALB/c mice subcutaneously. 11 days post-implantation, both tumours were injected with the indicated treatments (n=10 mice per group). Half of the animals were harvested 24 h post-injection (n=5), and the remaining animals were harvested at the 48 h post-injection timepoint. All tumours from the right flank were dissociated for flow cytometry analysis, while all tumours from the left flank were fixed in formalin and used in subsequent IHC. Following harvest, tumours were dissociated and analyzed by flow cytometry to detect VSVΔ51-infected at (b) 24 and (c) 48 h post-injection. Dissociated tumours were also analyzed for VV-infected cells at (d) 24 and (e) 48 h post-injection. (f) Gating strategy for analysis of infected cells in (b-e). (g-i) Following processing, sectioning, and staining of serial tumour sections with (g) anti-VSV antibody or (h) anti-VV antibody, slides were scanned and analyzed. Mask overlays indicate areas of infected cells (red), and counterstained non-infected cells (blue). Representative images shown. Quantification of DAB-positive (infected) area shown for (i) VSVΔ51. (mean ± SEM, $n = 4$ mice per group, P-value calculated by one-way ANOVA with Fisher's LSD test). Source data are provided as a Source Data file.

Supplementary Fig. 12

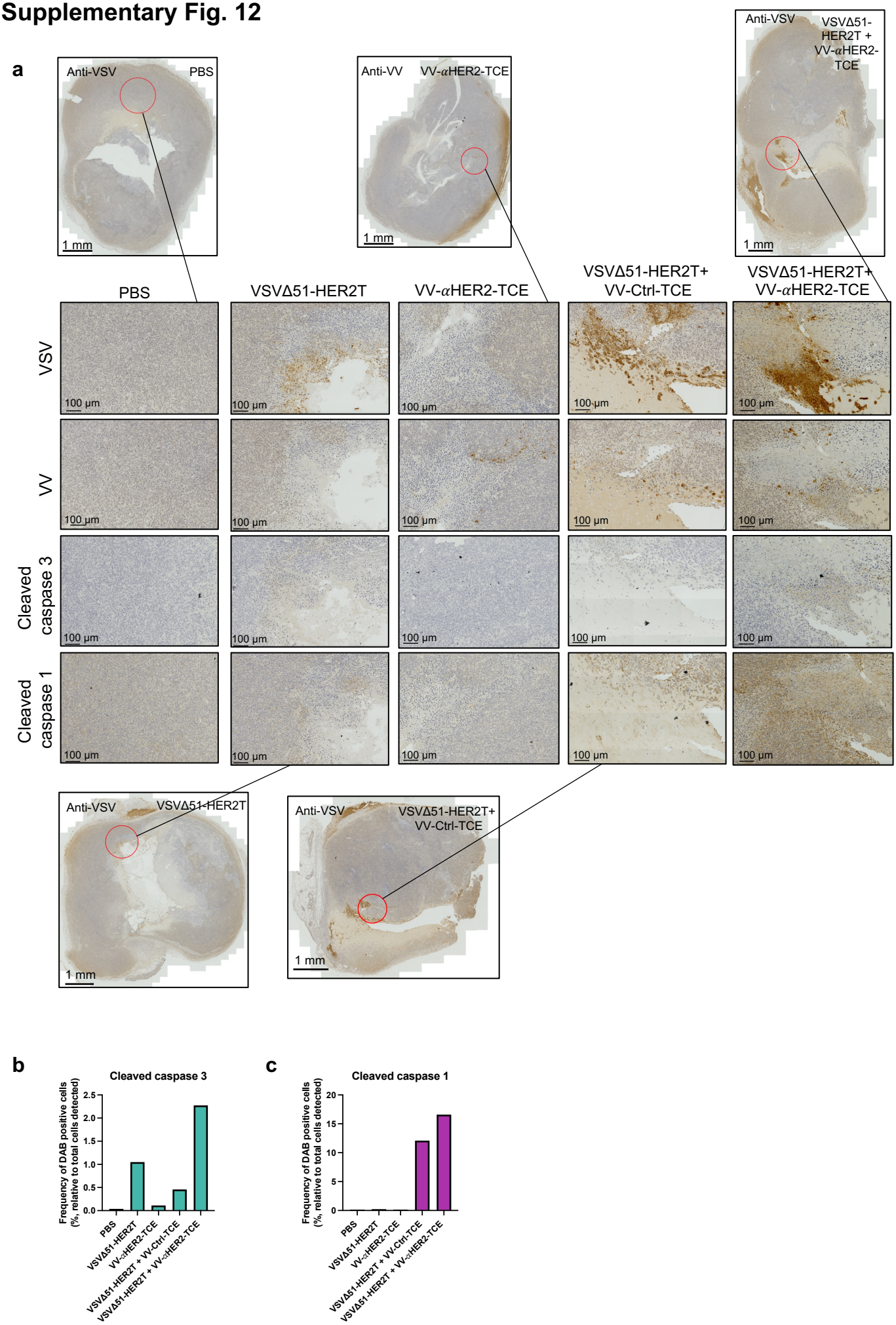

Supplementary Fig. 12: Injection of CT26 tumours with VSVΔ51-HER2T+ VV-*α*HER2-TCE triggers cell death in highly infected regions. Mice (n = 4 per group) bearing subcutaneous CT26 tumours were given a single intratumoural injection of the indicated treatments (from Supplementary Fig. 11). Tumours collected 48 h post-injection were fixed, paraffin embedded, and sectioned. Serial tumour sections were stained with the indicated antibodies and scanned. (a) Representative images from different tumour sections, stained with each of 4 different antibodies, are shown with close-up images of specific regions of interest (ROI) indicated by red circles (~1.5 mm^2 , 10,000+ detected cells per ROI per sample). These ROI were analyzed for the frequency of (b) cleaved-caspase 3 positive cells and (c) cleaved caspase 1 positive cells. Source data are provided as a Source Data file.

Supplementary Fig. 13

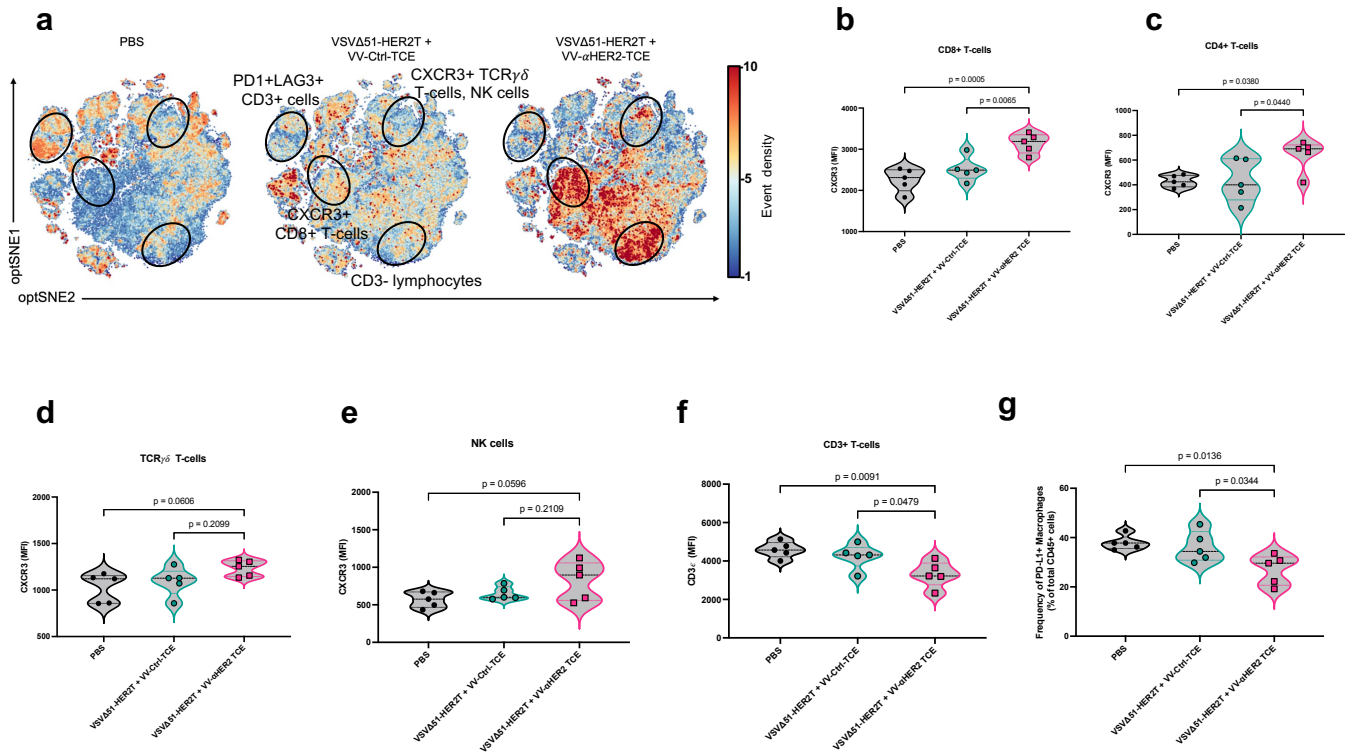

Supplementary Fig. 13: Intratumoural injection of VSVΔ51-HER2T + VV-*α*HER2-TCE enhances tumour-infiltrating lymphocyte activation. (a) Experimental overview: 5×10^5 CT26 cells were implanted s.c. in BALB/c mice in the right flank. Mice were treated i.t. as indicated. Tumours harvested and dissociated at day 5 were analyzed by flow cytometric analysis; data was subject to processing and dimensionality reduction using the optSNE algorithm; the clustering of each treatment group is displayed. Blue indicates rare events, while red indicates more frequent events as defined by the colour bar legend. (b-e) Levels of CXCR3 (MFI) were analyzed by flow cytometry in (b) CD8+ T-cells, (c) CD4+ T-cells, (d) TCR*γδ* T-cells, (e) and NK cells. (f) Quantification of CD3 levels (MFI). (g) Frequency of PD-L1+ macrophages relative to total CD45+ cells. (For all violin plots, mean ± SEM, $n = 5$ mice per group; *P*-value calculated by one-way ANOVA relative to VV-*α*HER2-TCE + VSVΔ51-HER2T, with Dunnett correction for multiple comparison.) Source data are provided as a Source Data file.

Supplementary Fig. 14

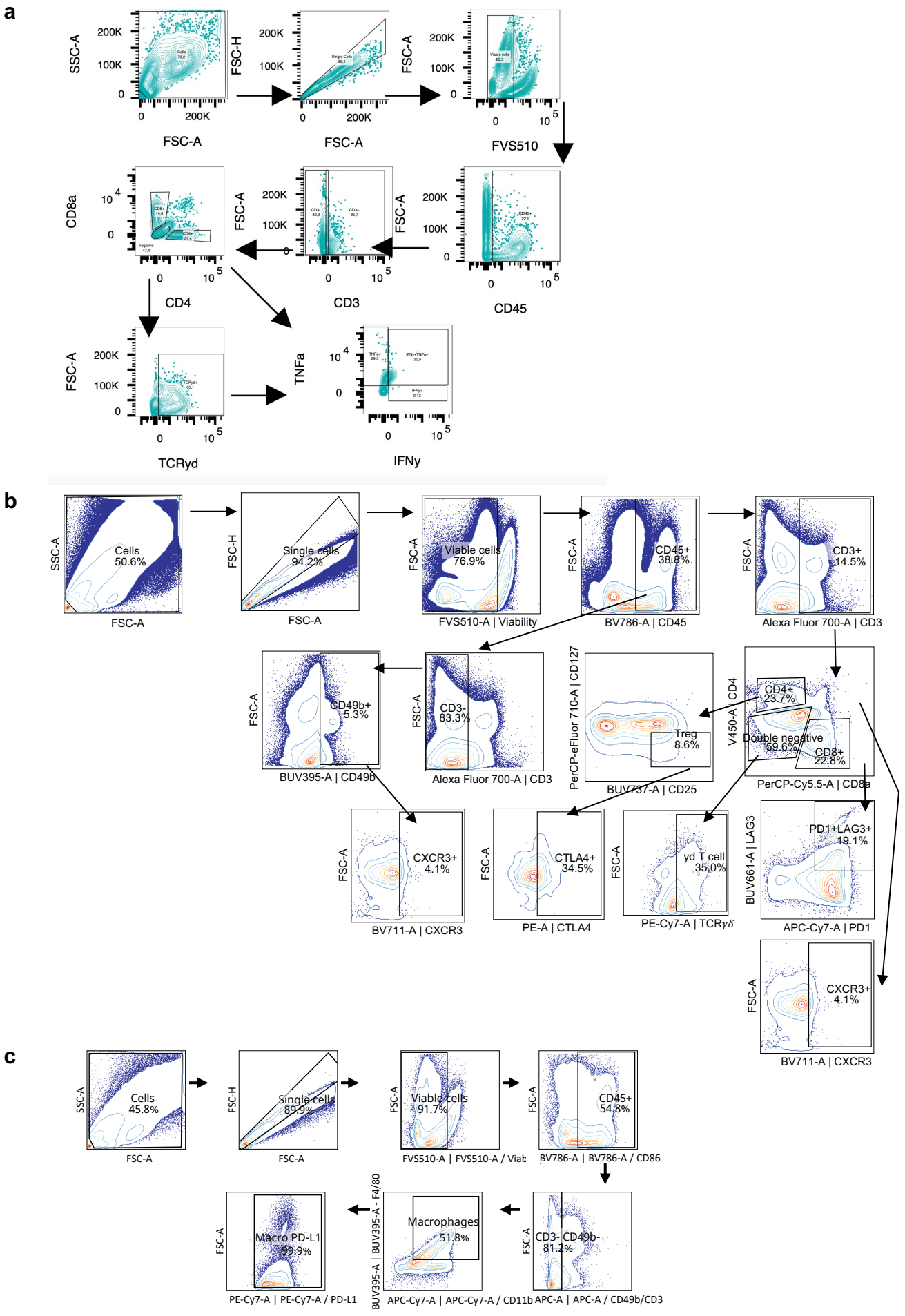

Supplementary Fig. 14: Gating strategies for flow cytometry. (a) Gating strategy for the intracellular staining of TNFα and IFNγ in Fig. 5 (b-d). (b) Gating strategy for the T-cell and NK cell staining of CXCR3 and PD-L1 in Fig. 5 (e-g) and Supplementary Fig. 13 (b-f). (c) Gating strategy for PD-L1+ macrophages in Supplementary Fig. 13 (g).

Supplementary Fig. 15

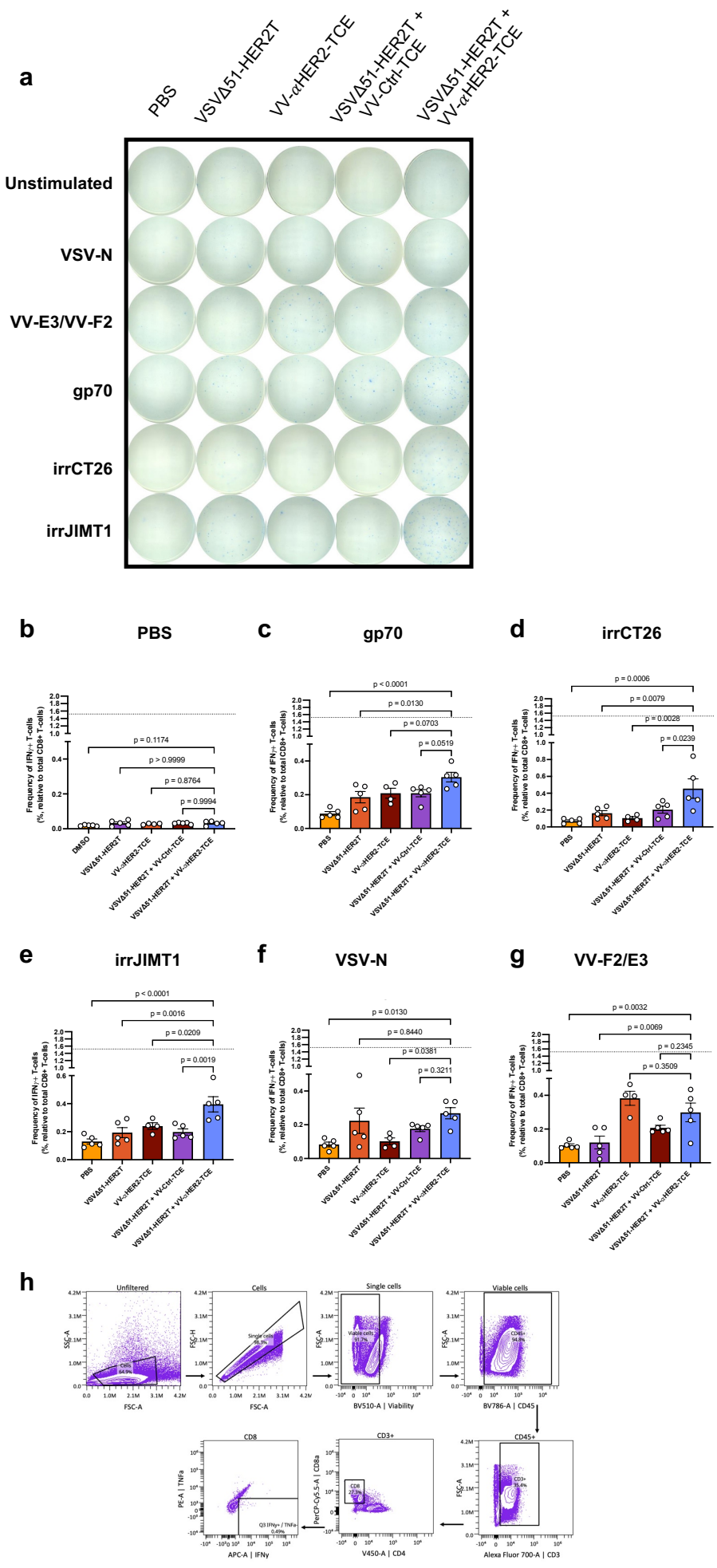

Supplementary Fig. 15: Splenocytes harvested from mice 14 days post-treatment exhibit reactivity against tumour and viral antigens. (a) Representative ELISpot wells from Fig. 5i-m. Following harvest of splenocytes from mice at day 14 post-treatment as indicated in Fig. 5h, splenocytes were used for intracellular cytokine staining (ICS). Splenocytes were analyzed by flow cytometric analysis for intracellular levels of IFNγ, following 24 h *ex vivo* culture (Golgi plugged) stimulated by (b) PBS control, (c) 10 μM gp70 peptide, (d) irradiated CT26 cells, (e) irradiated JIMT1 cells, (f) 10 μM VSV-N peptide, (g) 10 μM VV-F2/E3 peptides. Dotted lines indicate % IFNγ positive CD8+ T-cells following stimulation with PMA/ionomycin. (h) Gating strategy for quantifying IFNγ cells in (b-g). (mean ± SEM, n = 5 mice per group; P-value calculated by one-way ANOVA relative to VV-αHER2-TCE + VSVΔ51-HER2T, with Dunnett correction for multiple comparison.) Source data are provided as a Source Data file.

Supplementary Fig. 16

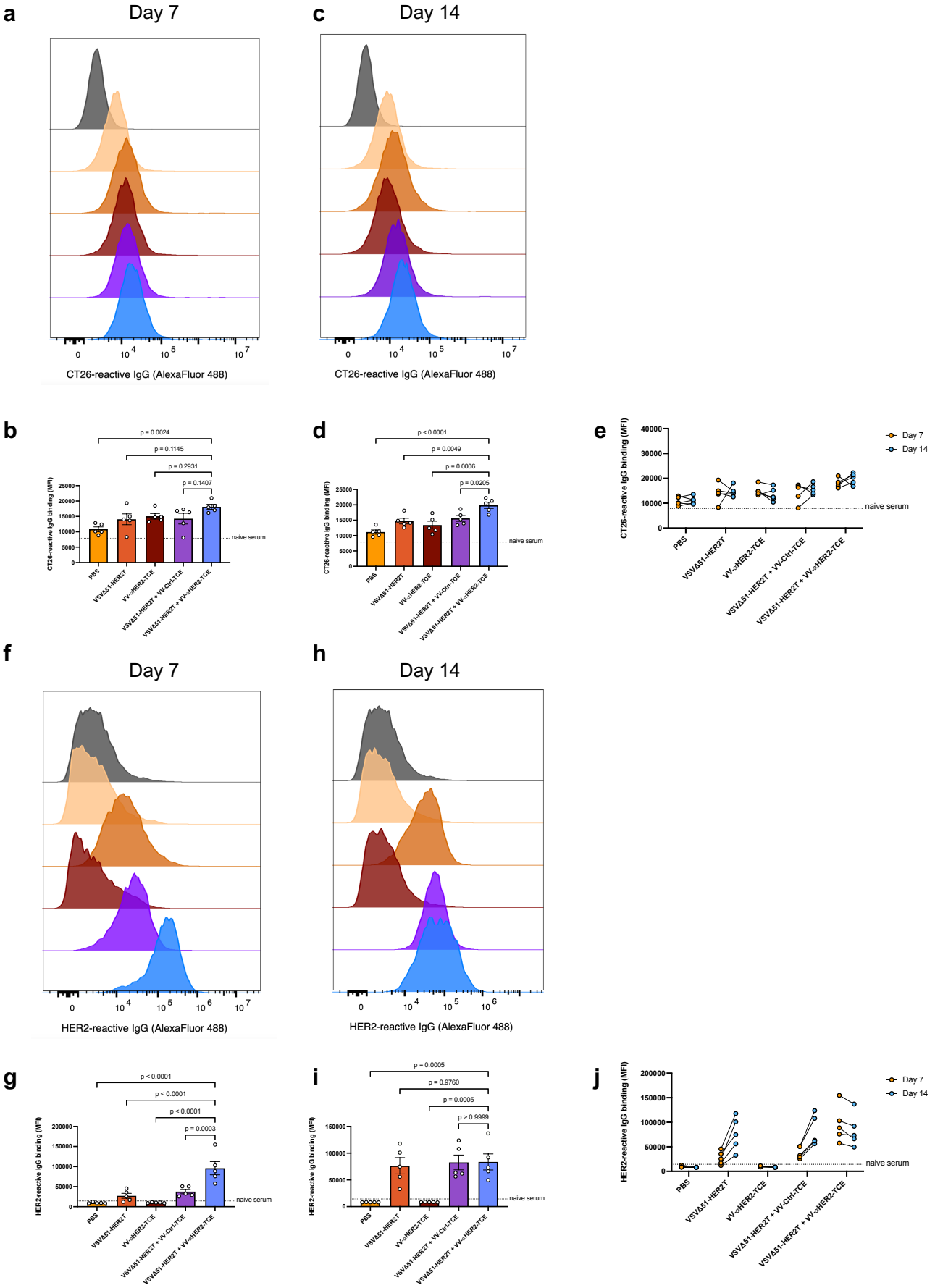

Supplementary Fig. 16: CT26 tumour-bearing mice receiving intratumoural VSVΔ51-HER2T+ VV-*α*HER2-TCE injections raise IgG against tumour and viral antigens. Serum was isolated from the lateral saphenous vein bleeds from Fig. 5 h at day 7 and day 14 post-treatment. Serum was diluted (1:100) and incubated with 5×10^5 cells as follows: (a-d) CT26 cells or (f-i) JIMT1 cells. Serum was washed off and IgG bound to cells was quantified using an anti-mouse IgG antibody (AlexaFluor™ Plus 488). Fluorescence signal was quantified by flow cytometry. (a-b, f-g) Serum collected at day 7; (c-d, h-i) serum collected at day 14. Change in the IgG reactivity between day 7 and 14 is plotted for (e) CT26 and (j) JIMT1. Dotted lines indicate signal obtained using serum from naïve mice. For all bar charts, mean ± SEM, $n = 5$ mice per group; *P*-value calculated by one-way ANOVA relative to VV-*α*HER2-TCE + VSVΔ51-HER2T, with Dunnett correction for multiple comparison. Source data are provided as a Source Data file.

Supplementary Fig. 17

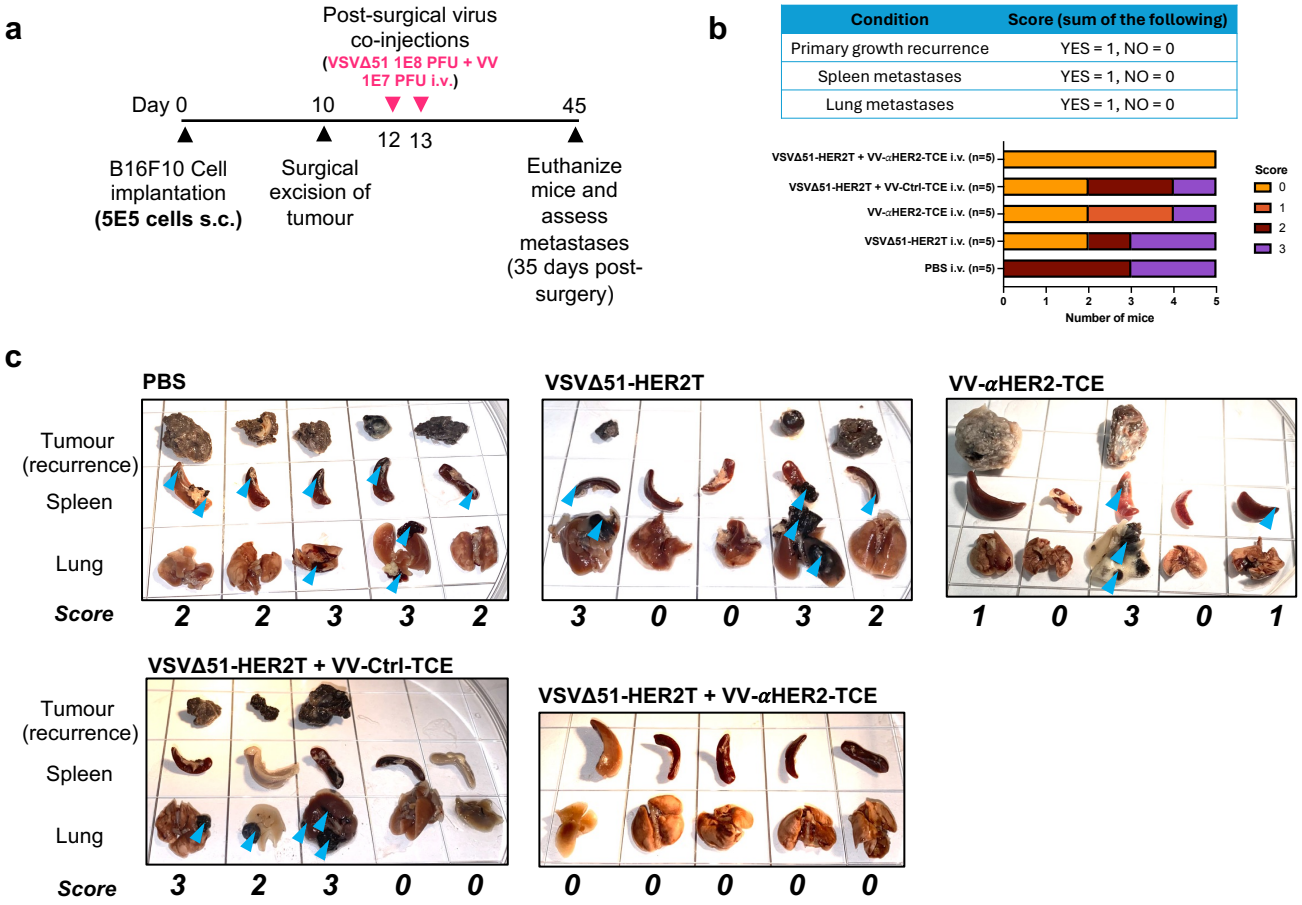

Supplementary Fig. 17: Treatment of C57BL/6 mice with VSVΔ51-HER2T + VV-αHER2-TCE following surgical excision of B16-F10 tumours prevents tumour recurrence and metastasis. (a) Experimental overview: 5×10^5 B16-F10 cells were implanted orthotopically in C57BL/6 mice subcutaneously in the right flank. 10 days post-implantation, tumours were excised, and mice received intravenous injections of the indicated treatments 48 h post-surgery. Mice were monitored over time and euthanized at day 45, where lungs, spleens, and recurrent primary tumours were harvested. (b) Mice were scored ($n = 5$ per group) as indicated. (c) Images of all recurrent primary tumours, spleens, and lungs. Blue arrows indicate black metastatic B16-F10 lesions within spleens and lungs. Numbers below the images indicate the score assigned. Source data are provided as a Source Data file.

Supplementary Table 1

Supplementary Table 1: Clinical characteristics of patient-derived tumour specimens.

Specimen	ID	TNM scoring	HER2 status	Pathology report
Ovarian 1	GTC306	N/A	Unknown	Ovarian mass with high grade carcinoma with mucinous differentiation and surface involvement
Ovarian 2	GTC269	PT3b, pN1a, pM1	Unknown	Dedifferentiated metastatic carcinoma with lymphovascular invasion. Left and right sides involved, including ovaries and fallopian tubes, and omentum.
Ovarian 3	GTC262	N/A	Unknown	Massive uterine fibroma extending from right ovary
Endometrial 1	GTC259	pT2, Nx, Mx	Unknown	Uterine carcinosarcoma, mixed Mullerian tumour, positive for cervical stromal, lymphovascular, and myometrial invasion.
Breast 1	GTC270	pT2, Nx, Mx	HER2-negative	Recurrent multifocal invasive ductal carcinoma, positive for lymphovascular invasion
Renal 1	GTC379	pT3a, N0, Mx	Unknown	Clear cell carcinoma WHO nucleolar grade 4/4. Highly necrotic ~70%, no lymph node involvement
Lung 1	GTC265	pT2b, N1, Mx	Unknown	Invasive adenocarcinoma, micropapillary predominant, minor acinar, and lepidic growth patterns. Lymphovascular invasion present.
Parotid 1	GTC344	pT3, N0, Mx	Unknown	Adenoid cystic carcinoma with focal high-grade transformation.
Parotid 2	GTC266	N/A	Unknown	Parotid mass, adenoma/indolent neoplasm

Supplementary Table 2

Supplementary Table 2: Clinical characteristics of patient-derived tumour specimens.

Specimen	ID	TNM scoring	HER2 status	Pathology report
Sarcoma	GTC409	pT2, pN0, pMx	Unknown	Pleomorphic sarcoma, high grade, dermis and subcutaneous fibroadipose tissue, no muscular or lymphovascular invasion, 75% necrotic tissue consistent with previous radiotherapy.
Colon	GTC411	pT3, N0, Mx	Unknown	Invasive colorectal adenocrcinoma, WHO low grade, G2 moderated differentiated
NSCLC	GTC413	pT1c, pN0, Mx	Unknown	Minimally-invasive non-mucinous adenocarcinoma; predominantly acinar. G1 well-differentiated, all margin uninvolved.
Ovarian	GTC414	pT1, Nx, Mx	Unknown	Left ovary endometroid adenocarcinoma, negative for surface involvement. Absence of malignancy in omentum, ascitic fluid, and right ovary. G2 moderated differentiated. P53 normal, MMR proficient.
Basal cell carcinoma	GTC415	pT3, N1, Mx	Unknown	Previous metastatic melanoma spread to left axillary lymph nodes. Axillary contents collected, 1/40 lymph nodes positive for malignancy.

Supplementary Table 3

Supplementary Table 3: Cell lines. * = The MC38 cell line was a generous gift from Dr. Guy Ungerechts; ** = The ID8-PP cell line was a generous gift from Dr. Iain McNeish; *** = The primary human ovarian cancer cell lines (AF2068, AF2028, AF2780) were obtained from the Ottawa Ovarian Ethics Board (OHSN-REB 1999540-01H) with informed consent, and provided by Dr. Barbara Vanderhyden; **** = 4T1.2 and 4T1.2-HER2 cells were a generous gift from Dr. Michael Kershaw; ‡ ,† † = These lines were generated as previously described. ATCC: American Type Culture Collection (Manassas, VA); DSMZ: Deutsche Sammlung von Mikroorganismen und Zellkulturen (Braunschweig, Germany); DMEM: Dulbecco's modified Eagle's medium (HyClone, Waltham, Massachusetts or Corning, Manassas, Virginia); RPMI: Roswell Park Memorial Institute medium (Hyclone, Cat. # SH3002701).

Cell line	Catalogue #	Host	Tissue origin	Classification	Growth medium	Source
Vero	CCL-81	African green monkey	Kidney	-	DMEM	ATCC
786-O	CRL-1932	Human	Kidney	Renal cell adenocarcinoma	DMEM	ATCC
GM38	GM00038	Human	Skin	Normal fibroblast	DMEM	Coriell Institute for Medical Research
HT29	HTB-38	Human	Colon	Colorectal adenocarcinoma	RPMI	ATCC
JIMT-1	ACC589	Human	Breast	Invasive ductal adenocarcinoma	DMEM	DSMZ
U-2 OS	HTB-96	Human	Bone	Osteosarcoma	RPMI	ATCC
HEK293T	CRL-3216	Human	Kidney	Embryonic kidney	DMEM	ATCC
AF2068	-	Human	Ovarian cancer ascites	Primary human ovarian cancer cells	RPMI	***
AF2028	-	Human	Ovarian cancer ascites	Primary human ovarian cancer cells	RPMI	***
AF2780	-	Human	Ovarian cancer ascites	Primary human ovarian cancer cells	RPMI	***
SKOV3	HTB-77	Human	Ovary	Ovarian adenocarcinoma	RPMI	ATCC
OVCAR-4	SCC258	Human	Ovarian cancer ascites	High grade serous carcinoma	RPMI	Millipore Sigma
J69 (Jurkat CD69-TdTomato)	-	Human	Lymphoblast	T cell leukemia	RPMI	‡
CT26.WT (CT26)	CRL-2638	Mouse (BALB/c)	Colon	Colon adenocarcinoma	DMEM	ATCC
CT26-HER2T	-	Mouse (BALB/c)	Colon	Colon adenocarcinoma	DMEM	††
MC38	-	Mouse (C57BL/6)	Colon	Colon adenocarcinoma	DMEM	*
MC38-HER2T	-	Mouse (C57BL/6)	Colon	Colon adenocarcinoma	DMEM	††
ID8 (Tp53-/- Pten-/-)	-	Mouse (C57BL/6)	Ovary	High-grade serous carcinoma	DMEM supplemented with 4% FBS and 1% ITSS (5 µg/mL insulin, 5 µg/mL transferrin, and 5 ng/mL sodium selenite; R&D Systems, MN, USA, Cat. # AR013).	**
ID8-PP-HER2T	-	Mouse (C57BL/6)	Ovary	High-grade serous carcinoma		††
ID8-HER2T	-	Mouse (C57BL/6)	Ovary	High-grade serous carcinoma		††
4T1.2	CRL-3406	Mouse (BALB/c)	Breast	Breast adenocarcinoma	RPMI	ATCC, ****
4T1.2-HER2	-	Mouse (BALB/c)	Breast	Breast adenocarcinoma	RPMI	****
4T1.2-HER2T	-	Mouse (BALB/c)	Breast	Breast adenocarcinoma	RPMI	††
B16-F10	CRL-6475	Mouse (C57BL/6)	Skin	Melanoma	RPMI	ATCC

Supplementary Table 4

Supplementary Table 4: Antibodies used for flow cytometry.

Antibody	Cat. #	Clone	Dilution
CD45-BV786	BD, 564225	30-F11	1:1000
CD3ϵ-Alexa Fluor 700	BD, 561805	SP34-2	1:300
CD49b-BUV395	BD, 740250	HMα2	1:100
CD335-BUV805	BD, 742066	29A1.4	1:100
CD314-BUV496	BD, 750014	9C11G4	1:100
CD4-V450	BD, 560468	RM4-5	1:1000
CD8α-PerCP-Cy5.5	BD, 551162	53-6.7	1:200
TCR γ/δ-PE-Cy7	Invitrogen, 25-5711-82	eBioGL3 (GL-3, GL-3)	1:200
CD25-BUV737	Invitrogen, 367-0251-82	PC61.5	1:100
CD69-BUV605	BD, 563290	H1.2F3	1:100
PD-1-APC-Cy7	Biolegend, 135223	29F.1A12	1:100
LAG3-BUV661	BD, 741594	C9B7W	1:100
CTLA-4-PE	Invitrogen, 12-1522-82	UC10-4B9	1:200
CD127-PerCP-eFluor 710	Invitrogen, 46-1273-82	eBioSB/199 (SB/199)	1:200
CD62L-NovaFluor Blue 555	Invitrogen, M006T02B03	MEL-14	1:300
CD44-APC	BD, 563058	IM7	1:100
CXCR3-BV711	BD, 740825	CXCR3-173	1:100
CD103-BV421	Biolegend, 121421	2E7	1:100
CD39-PE-Fire 640	Biolegend, 143817	Duha59	1:100
CD27-BV650	BD, 740491	LG.3A10	1:200
CD3ϵ-APC	Biolegend, 100235	17A2	1:200
CD49b-APC	Biolegend, 108909	DX5	1:200
CD19-PE-Cy5	Biolegend, 115509	6D5	1:200
CD11c-PE	BD, 553802	HL3	1:100
CD11b-APC-Cy7	Biolegend, 101225	M1/70	1:100
F4/80-BUV395	BD, 565614	T45-2342	1:200
MHCII (IA-IE)-BUV737	Invitrogen, 367-5321-82	M5/114.15.2	1:500
CD86-APC-R700	BD, 565479	GL1	1:200
PD-L1-PE-Cy7	Biolegend, 124313	10F.9G2	1:100
CD205-SB600	Invitrogen, 63-2051-82	205yekta	1:200
CD1d-BV711	BD, 740711	1B1	1:100
IFNγ-APC	Invitrogen, 17-7311-82	XMG1.2	1:100
TNFα-PE	Biolegend, 506305	MP6-XT22	1:100
Trastuzumab (1^0)	Herceptin®; Hoffman-La Roche, Mississauga, Ontario, Canada	N/A; Clinical grade	1:1000
Anti-human IgG-PE (2^0)	Invitrogen, PA1-86078	N/A; RRID: AB_933621	1:300
Anti-mouse IgG-AlexaFluor 488	Invitrogen, A32723	N/A; RRID: AB_2633275	1:300